View metadata, citation and similar papers at core.ac.uk

brought to you by CORE

provided by Archivio istituzionale della ricerca - Università di Brescia

Traffic 2006; **7:** 1–13
Blackwell Munksgaard

© 2006 The Authors

doi: 10.1111/j.1600-0854.2006.00481.x

Defective Intracellular Trafficking of Uromodulin Mutant Isoforms

Ilenia Bernascone[1,†], Stefano Vavassori[1,†], Alessio Di Pentima[2], Sara Santambrogio[1], Giuseppe Lamorte[3], Antonio Amoroso[4], Francesco Scolari[5], Gian Marco Ghiggeri[6], Giorgio Casari[7], Roman Polishchuk[2] and Luca Rampoldi[1,*]

[1]*Dulbecco Telethon Institute, DIBIT, San Raffaele Scientific Institute, Via Olgettina 58, 20132 Milan, Italy*
[2]*Department of Cell Biology and Oncology, Istituto di Ricerche Farmacologiche Mario Negri, Via Nazionale, 66030 Santa Maria Imbaro, Chieti, Italy*
[3]*Biotechnology and Biosciences Department, University of Milan Bicocca, Piazza della Scienza 2, 20126 Milan, Italy*
[4]*Department of Genetics, Biology and Biochemistry, University of Turin, Via Santena 19, 10126 Turin, Italy*
[5]*Division of Nephrology, Spedali Civili and University of Brescia, Piazzale Spedali Civili 1, 25125 Brescia, Italy*
[6]*Laboratory on Pathophysiology of Uremia, G. Gaslini Institute, L.go G. Gaslini 5, 16147 Genoa, Italy*
[7]*Human Molecular Genetics Unit, DIBIT, San Raffaele Scientific Institute, Via Olgettina 58, 20132 Milan, Italy*
**Corresponding author: Luca Rampoldi, rampoldi.luca@hsr.it*
[†]*These authors contributed equally to this work*

Medullary cystic kidney disease/familial juvenile hyperuricemic nephropathy (MCKD/FJHN) are autosomal dominant renal disorders characterized by tubulo-interstitial fibrosis, hyperuricemia and medullary cysts. They are caused by mutations in the gene encoding uromodulin, the most abundant protein in urine. Uromodulin (or Tamm–Horsfall protein) is a glycoprotein that is exclusively expressed by epithelial tubular cells of the thick ascending limb of Henle's loop and distal convoluted tubule. To date, 37 different uromodulin mutations have been described in patients with MCKD/FJHN. Interestingly, 60% of them involve one of the 48 conserved cysteine residues. We have previously shown that cysteine-affecting mutations could lead to partial endoplasmic reticulum (ER) retention. In this study, as a further step in understanding uromodulin biology in health and disease, we provide the first extensive study of intracellular trafficking and subcellular localization of wild-type and mutant uromodulin isoforms. We analyzed a set of 12 different uromodulin mutations that were representative of the different kind of mutations identified so far by different experimental approaches (immunofluorescence, electron microscopy, biochemistry and *in vivo* imaging) in transiently transfected HEK293 and Madin–Darby canine kidney cells. We assessed protein processing in the secretory pathway and could demonstrate that although to different extent, all uromodulin mutations lead to defective ER to Golgi protein transport, suggesting a common pathogenetic mechanism in MCKD/FJHN.

Key words: chronic renal diseases, ER retention, familial juvenile hyperuricemic nephropathy, medullary cystic kidney disease, protein trafficking, Tamm–Horsfall protein, uromodulin

Received 30 April 2006, revised and accepted for publication 26 July 2006

Uromodulin is the most abundant protein in human urine under physiological conditions, being excreted at a rate of 50–100 mg per day (1). It was initially characterized by Tamm and Horsfall in 1950 (2), and it is also referred to as Tamm–Horsfall protein. Uromodulin is found in urine as a high-molecular-weight polymer (M_r 1–10 $\times$ 10^6) that can be dissociated into monomers of about 95 kDa (3). It is a glycoprotein with seven out of eight potential N-glycosylation sites being glycosylated; N-glycans account for about 25% of its molecular weight (4). Uromodulin is exclusively detected in epithelial cells of the thick ascending limb (TAL) of the loop of Henle and in distal convoluted tubules (DCT) (1). It is membrane bound via a glycosyl phosphatidylinositol (GPI) anchor, and it is released into the tubular lumen from kidney tubular cells through a proteolytic cleavage by a yet to be identified protease (5). GPI-anchored uromodulin is mainly localized at the apical plasma membrane of epithelial tubular cells (6).

Despite being extensively studied in the past 50 years, uromodulin biological function has not been fully elucidated. Based on its specific localization in the TAL and DCT, the 'diluting' tracts of the nephron and its ability to polymerize *in vitro* to form a gel-like structure that is water impermeable and allows ion movement (7), it has been proposed that uromodulin has a role in salt transport and is important for water impermeability of the TAL, a process that is crucial for urine concentration. Recent results demonstrated that urinary uromodulin has a protective role against urinary tract infections and nephrolithiasis. In particular, *umod* knock-out mice have been shown to be more susceptible to infections by type 1 fimbriated *Escherichia coli* (8,9), *Klebsiella pneumoniae* and *Staphylococcus saprophyticus* (10). Furthermore, $umod^{-/-}$ mice show spontaneous formation of calcium crystals in the kidney that is dramatically increased after a diet supplemented with ethylene glycol, an oxalate precursor, and vitamin D3, which enhances calcium absorption (11). Moreover, uromodulin can directly activate dendritic cells via the Toll-like receptor-4 pathway (12), suggesting that this protein may play an important role in innate immune response in the kidney (13).

Mutations in uromodulin gene *UMOD* cause medullary cystic kidney disease (MCKD) and familial juvenile hyperuricemic nephropathy (FJHN), two autosomal dominant diseases characterized by alteration of urinary concentrating ability, tubulo-interstitial fibrosis, hyperuricemia and gout and progressive kidney failure frequently leading to end-stage renal disease and dialysis (14). Furthermore, two mutations have been described in patients affected by glomerulocystic kidney disease (GCKD) (15,16), characterized by cyst dilatation and collapse of glomeruli. Including the new mutation here described, 38 *UMOD* mutations have been reported (14–25); the majority of them are clustered in exons 4 and 5 and localized in the N-terminal half of the protein. The vast majority of the reported mutations (35) are missense changes mainly affecting (more than 50% of the cases) one the 48 conserved cysteine residues. The remaining three mutations are in-frame deletions extending from 5 to 33 amino acids.

We have previously reported a preliminary functional study of four cysteine-affecting uromodulin mutations (C148W, C150S, C315R and C317Y), showing that mutant protein trafficking to the cell plasma membrane was impaired in transiently transfected HEK293 due to partial endoplasmic reticulum (ER) retention (15). These results were consistent with immunohistochemistry on patient's kidney biopsies, showing the presence of intracellular uromodulin aggregates (15,19), and with Western blot analysis of urinary protein, demonstrating a dramatic uromodulin reduction in patient urine.

In this study, as a further step in understanding uromodulin biology in health and disease, we provide the first extensive study of intracellular trafficking and subcellular localization of wild-type (wt) and mutant isoforms. We analyzed a set of different uromodulin mutations that were representative of the different kind of mutations identified so far by transiently transfecting two kidney cell lines and using different experimental approaches [immunofluorescence, electron microscopy (EM), biochemistry and live imaging]. We could demonstrate that mutant uromodulin trafficking is impaired in all the mutants studied, showing ER to Golgi trafficking delay although different mutations affect trafficking to different extents.

Results

Uromodulin mutations alter protein trafficking to the plasma membrane

Uromodulin contains a N-terminal signal peptide, three epidermal growth factor (EGF)-like domains between positions 31 and 148 and a fourth potential EGF-like domain at positions 281–336, a central domain of unknown function containing eight conserved cysteine residues (D8C) at positions 171–276 (26), a zona pellucida (ZP) domain from amino acids 336 to 585 and a GPI anchor attachment site at position 614 (Figure 1A). EGF-like domains are almost invariably found in a variety of secreted proteins or in the extracellular domain of membrane-bound proteins and are likely involved in protein–protein interactions. The ZP domain is responsible for protein polymerization into 10–15 nm fibers (27).

Among the 38 *UMOD* mutations reported so far, we focused on missense mutations identified in families with MCKD/FJHN and GCKD. This study includes a newly identified mutation (P236R, 707C>G) that was found in the affected members of a FJHN Italian family (Brugnano and Scolari, personal communication). A mutation at the same nucleotide (707C>T), resulting in the same proline residue being exchanged for a leucine (P236L), was previously reported (22). The 12 analyzed mutations (highlighted in Figure 1A) are localized in the EGF-like domains [D59A(19), N128S(18), C148W(15), C315R(15) and C317Y(15)], in the central portion of the protein [C150S(15)], including the D8C domain [R204G(19), C217R(14), T225K(21), M229R(20) and P236R], or in the ZP domain [C347G (23)].

All the studied mutations are predicted to affect protein stability when analyzed with different prediction programs [SIFT (28), PMUT (29) and MUPRO (30)] although to different extents (Figure 1C).

To assess the effect of different uromodulin mutations on protein trafficking, we performed transient transfection experiments in HEK293 cells that do not express uromodulin. We transfected equal amounts of constructs and verified equal transfection efficiency by cotransfection with an enhanced green fluorescent protein (EGFP)-expressing plasmid. Equal amount of total uromodulin produced in mutant and wt transfected cells was verified by Western blot analysis (Figure S1). We quantified the number of transfected cells exposing uromodulin on the plasma membrane by fluorescent-activated cell sorter (FACS) analysis 14 h after transfection. Interestingly, the majority of mutants showed a reduction in the number of positive cells, suggesting that mutations lead to a delay of uromodulin transport to the plasma membrane although this effect varied from a 25% reduction in M229R to a 75% one in N128S (Figure 1B). The same effect could be obtained in wt transfected cells that were cultured in reducing conditions (DTT, 1 and 2 mM). Mutants T225K, C317Y and C347G did not significantly differ from the wt at this time-point after transfection. However, a reduction in the number of positive cells could be observed for these mutants at shorter time (4 and 6 h) after transfection (data not shown). Moreover, these mutants revealed a trafficking defect when studied by other experimental approaches (see below).

Mutant uromodulin is retained in the ER

To assess if trafficking impairment of the different uromodulin mutant isoforms was due to ER retention, as already demonstrated for the cysteine-affecting mutants, we

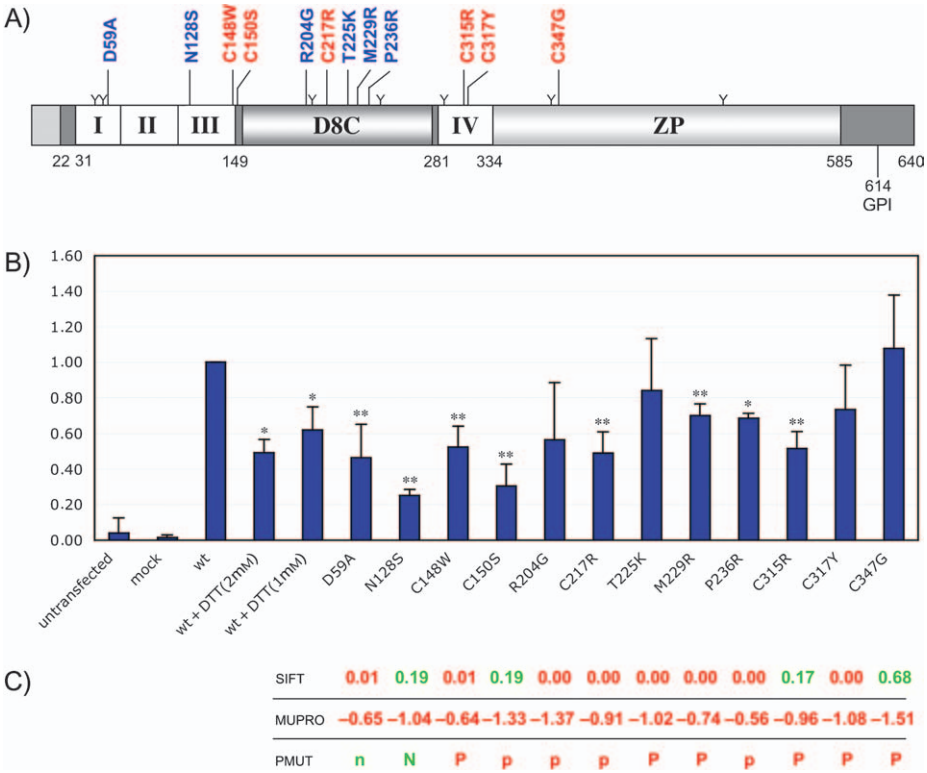

Figure 1: Fluorescence-activated cell sorter analysis of uromodulin-positive HEK293 cells transiently transfected with either wild type or mutant uromodulin isoforms. A) Schematic representation of uromodulin domain organization. Leader peptide is shown as a dotted box and EGF-like domains are shown as numbered white boxes. Positions of the D8C domain, ZP domain and the GPI-anchor attachment site are indicated. The seven glycosylation sites are marked as Y. The position and description of the 12 uromodulin mutations that were analyzed in this study are shown. B) FACS analysis of HEK293 cells transfected with either wt or mutant constructs and positive for membrane-bound uromodulin on the cell surface. Cells were collected 14 h after transfection. Data are normalized for transfection efficiency (by cotransfecting with an EGFP-expressing plasmid) and to wt. Average percentage values for five replicates are shown. *, $p < 0.05$; **, $p < 0.01$ (Mann–Whitney two-tailed test). Bars represent ±SD. C) Results of the predicted effect of uromodulin mutations as assessed by using SIFT, MUPRO and PMUT programs. Scores in each column are relative to the mutation indicated above. For SIFT analysis, scores below 0.05 are predicted to be deleterious. In MUPRO analysis, the predicted relative stability change $\Delta\Delta G$ is given; a negative value predicts that the mutation is destabilizing. For PMUT analysis, pathological (P) and neutral (N) predicted effects are indicated; statistically significant scores (confidence index above 5, in a range from 0 to 9) are in upper case. For all programs, scores predicting a pathological effect are in red and permissive ones are in green.

analyzed the intracellular distribution of wt and mutant uromodulin in transiently transfected HEK293 cells at different times after transfection. We carried out immunofluorescence analysis on permeabilized cells at 4 and 6 h after transfection. In wt transfected cells, intracellular uromodulin signal was mainly localized in the Golgi apparatus as shown by colocalization with giantin (Figure 2). On the contrary, mutant isoforms showed an intracellular reticular-like staining that mainly colocalized with calreticulin, an ER resident protein (Figures 2, S2A,B and S3A,B). These results suggest that all uromodulin mutations that were studied lead to defective trafficking of mutant protein to the plasma membrane due to ER retention. Consistently, uromodulin plasma membrane signal was reduced in mutant transfected cells (Figure S4). Besides this common effect, some mutations show a more severe cellular phenotype than others. For this reason, we selected for the experiments that are reported hereafter a subset of representative mutations affecting protein trafficking to different extent (C150S>T225K>C347G). To better quantify the difference in intracellular protein distribution that was observed in immunofluorescence experiments, we carried out EM analysis on transiently transfected cells 6 h after transfection and assessed the distribution of uromodulin in different cell compartments (Figure 3). Wt protein was mainly localized at the plasma membrane (60%); intracellular protein was predominantly found in the Golgi apparatus stacks (30%). On the contrary, the vast majority of mutant protein (C150S and T225K mutants in Figure 3) was detected in the ER (75% and 85%, respectively), whereas only a minor fraction (about 4% in both mutants) was localized at the plasma membrane. This effect could also be observed for mutant C347G although to a minor extent (Figure 3).

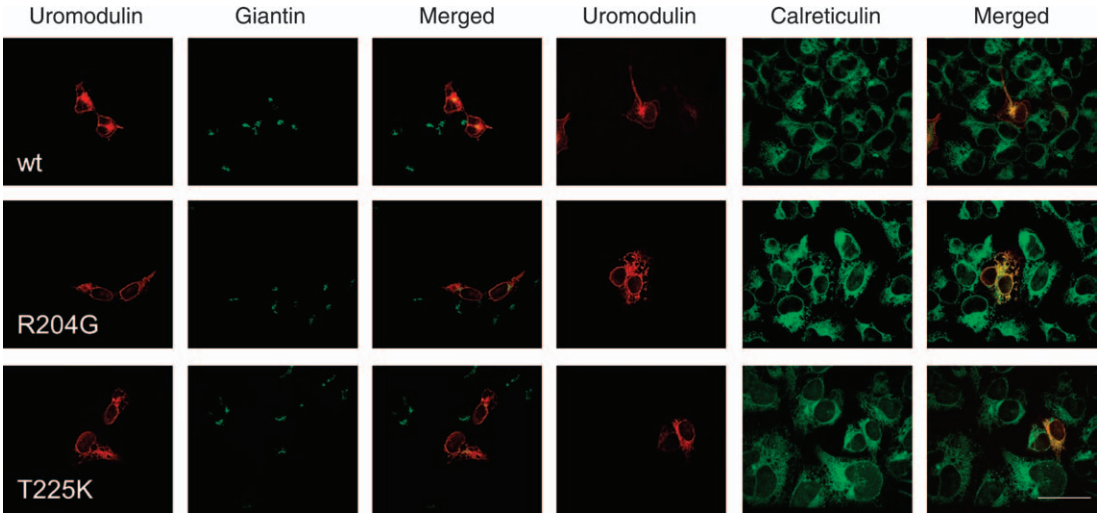

Figure 2: Immunofluorescence analysis showing intracellular distribution of wt and mutant uromodulin in transiently transfected HEK293 cells. Cells were transfected, methanol fixed 6 h after transfection and incubated with anti-uromodulin and either anti-giantin (Golgi marker) or anti-calreticulin (ER marker) antibodies. Wt uromodulin is mainly localized to the Golgi apparatus, while mutant protein is mainly localized in the ER. Bar = 35 μm.

We assessed by fluorescence recovery after photobleaching (FRAP) experiments if the defective trafficking of mutant protein was indeed caused by delayed exit from the ER or/and by defective protein transport from the *trans* Golgi network (TGN) to the plasma membrane. Madin–Darby canine kidney (MDCK) cells were transiently transfected with wt and mutant EGFP-fused uromodulin constructs. We verified that EGFP fusion did not significantly alter trafficking properties of uromodulin isoforms by immunofluorescence and Western blot (by checking ratios of mature versus precursor protein in soluble and insoluble fractions) experiments (data not shown). FRAP studies revealed that mutant transfected cells (C150S and C347G shown in Figures 4 and 5) showed a significantly reduced total fluorescence recovery (35% and 54%, respectively) in the Golgi area 20 min after photobleaching when compared with wt (81%) (Figures 4 and 5; Movies S1–3). By using the same experimental approach, no TGN to plasma membrane trafficking defect could be observed in mutant transfected cells when compared with wt (Figure 6; Movies S4–6). The decreased fluorescence recovery at the Golgi after photobleaching demonstrates that defective trafficking of mutant uromodulin isoforms is due to a delayed exit from the ER.

Transport of uromodulin mutants through the Golgi apparatus is not impaired

To assess if uromodulin mutations could also affect protein transit through the Golgi, thereby altering protein glycosylation and the ratio of immature to mature protein, we carried out Western blot analyses on transiently transfected HEK293 cells. Uromodulin is present as a precursor form of 85 kDa and a mature form of about 100 kDa. In wt transfected cells, the two bands are similarly distributed in the soluble fraction, whereas the 100-kDa band is greatly enriched in the insoluble fraction (Figure 7A). On the contrary, all mutants (Figures 7A and S1) are enriched both in the soluble and in the insoluble fraction in the low-molecular-weight band. To assess the oligosaccharide modifications of the two uromodulin isoforms, cell lysates were treated with two deglycosidases, endo-β-*N*-acetylglucosaminidase H (Endo H) and peptide-N-glycosidase F (PNGase F). While PNGase F can hydrolyze all types of *N*-linked glycans of glycoproteins, Endo H cleaves only high-mannose oligosaccharides of ER glycoproteins, but it does not cleave Golgi-modified glycoproteins. PNGase F cleaves both uromodulin isoforms to a 60 kDa one, which corresponds to the deglycosylated protein. On the contrary, Endo H cleaves the 85 kDa form only (Figure 7B,C), thereby indicating that it corresponds to an uromodulin precursor in the ER. These results are consistent with ER retention of mutant uromodulin. Moreover, the different ratio of immature to mature form of protein in the soluble fraction is consistent with the different extent of trafficking impairment for the studied mutations that was observed by other experimental approaches.

Transiently transfected HEK293 cells were treated with Phosphatidylinositol-specific phospholipase C (Pi-PLC), a lipase that hydrolyzes the phosphate bond in the GPI anchor, therefore releasing GPI-anchored membrane proteins from the cell surface, before preparing protein extracts (Figure 8A). Both wt and mutant protein are cleaved by Pi-PLC, suggesting that mutations do not affect uromodulin GPI anchoring. Most of the proteins that are released by Pi-PLC treatment correspond to the 100-kDa mature form present in the insoluble fraction. Endo H and

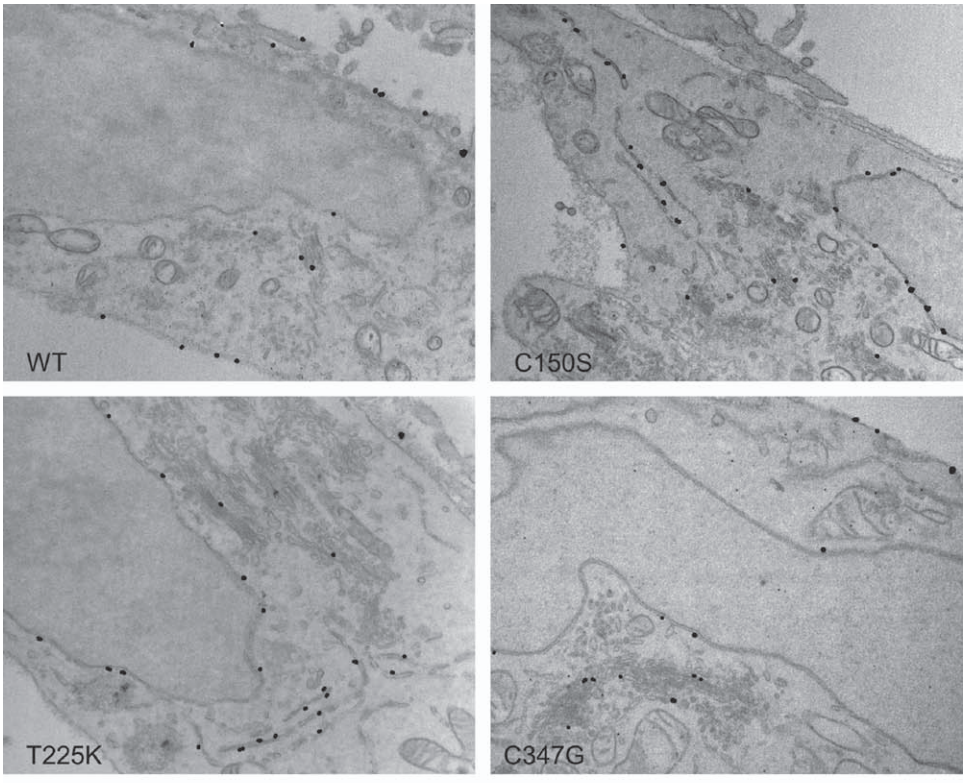

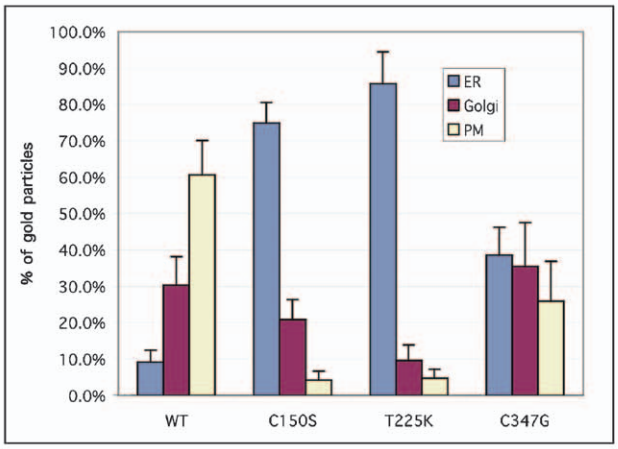

	ER	Golgi	PM
WT	9.1%	30.3%	60.6%
C150S	75.0%	20.8%	4.2%
T225K	85.7%	9.5%	4.8%
C347G	38.6%	35.5%	25.9%

Figure 3: Immuno-EM analysis of HEK293 cells transiently transfected with either wt or mutant uromodulin isoforms. Cells were fixed 6 h after transfection. Quantification of gold particles residing within different compartments of the secretory pathway is shown. While wt uromodulin is mainly on the plasma membrane and in the Golgi, most of mutant proteins are retained in the ER. Bars represent ±SD.

PNGase F assays clearly show that both wt and mutant Pi-PLC-released uromodulin isoforms are fully glycosylated (Figure 8B), suggesting that uromodulin mutations do not alter protein modification in the Golgi apparatus. The same result could be obtained when analyzing wt and mutant protein released in the culture medium (data not shown).

Discussion

This study provides the first extensive functional analysis on 12 different uromodulin mutations, showing for the first time that different mutations lead to a common trafficking defect of the mutated protein, thereby suggesting

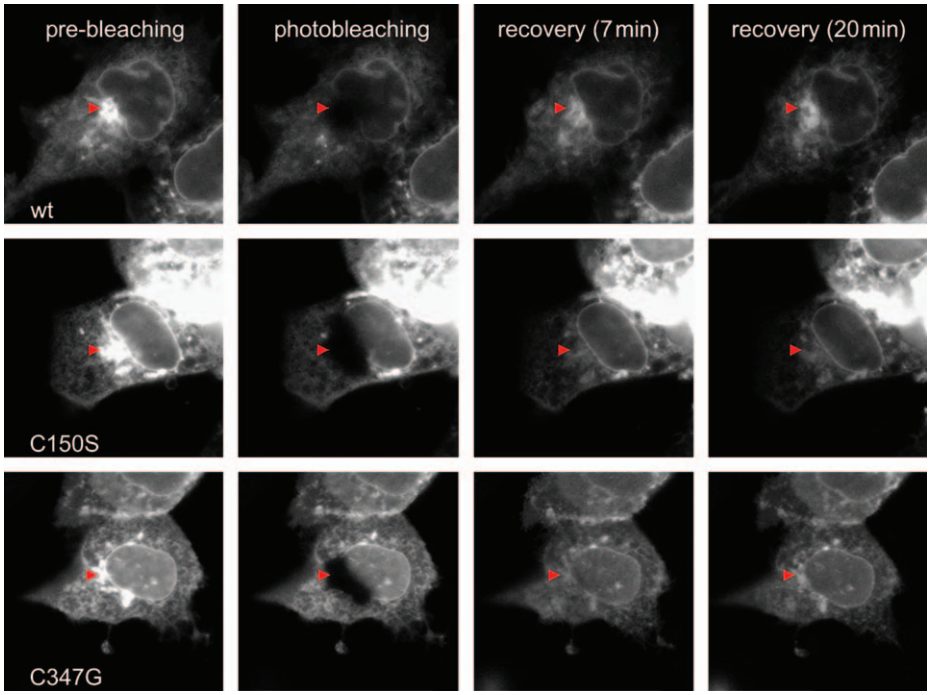

Figure 4: Time-lapse imaging of MDCK cells transiently transfected with either wt or mutant EGFP–uromodulin constructs. FRAP in the Golgi apparatus region is shown (arrowheads).

a common pathogenetic mechanism in uromodulin storage diseases.

Including the new mutation P236R described here, 38 different *UMOD* mutations have been reported so far in families with MCKD/FJHN and GCKD, comprising 35 missense mutations and three in-frame deletions. Interestingly, more than half of the mutations (21) affect one of the 48 conserved cysteine residues that are believed to be engaged in the formation of 24 intramolecular disulphide bonds (31). Cysteine-affecting mutations are therefore likely to alter disulphide bonds pattern and hence protein structure. Other mutations that could affect protein folding are: G103C, V93_G97del4ins, E188del33, changes that likely affect the disulfide bond pattern by inserting/deleting cysteine residues and N128S, which is predicted to be part of the calcium co-ordinating site in EGF-like domain III (18). Indeed, by affecting calcium binding, this mutation could destabilize the EGF-like domain conformation and increase interdomain flexibility (32). The effect of the other reported mutations is more difficult to be predicted.

To assess if different mutations in uromodulin could lead to a common effect on protein intracellular trafficking, we studied a panel of mutations that are representative of the different *UMOD* mutations known so far. In particular, we chose mutations that are localized in the EGF-like domains (D59A, N128S, C148W), including putative EGF-like IV (C315R, C317Y), in the central part of the protein (C150S), comprising the D8C domain (R204G, C217R, T225K, M229R and P236R), or in the ZP domain (C347G). All mutations but one (D59A) affect amino acid residues that are conserved in the mouse, rat, dog and

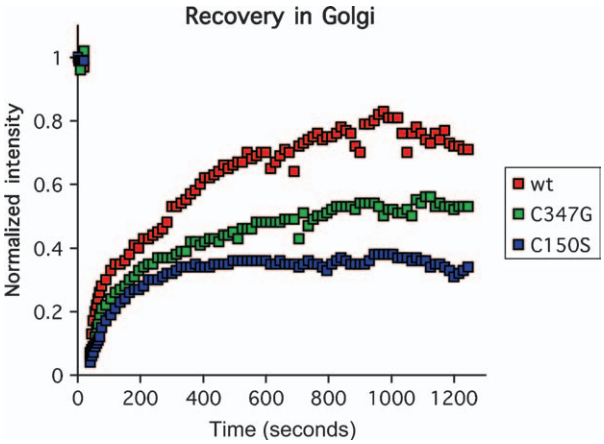

Figure 5: FRAP in the Golgi apparatus area in MDCK cells transiently transfected with either wt or mutant EGFP–uromodulin constructs. Average fluorescence intensities within the region of interest are shown (time-points every 5 seconds). Although to different extent, uromodulin mutants show a significant reduction in the fluorescence recovery, suggesting an ER to Golgi trafficking defect.

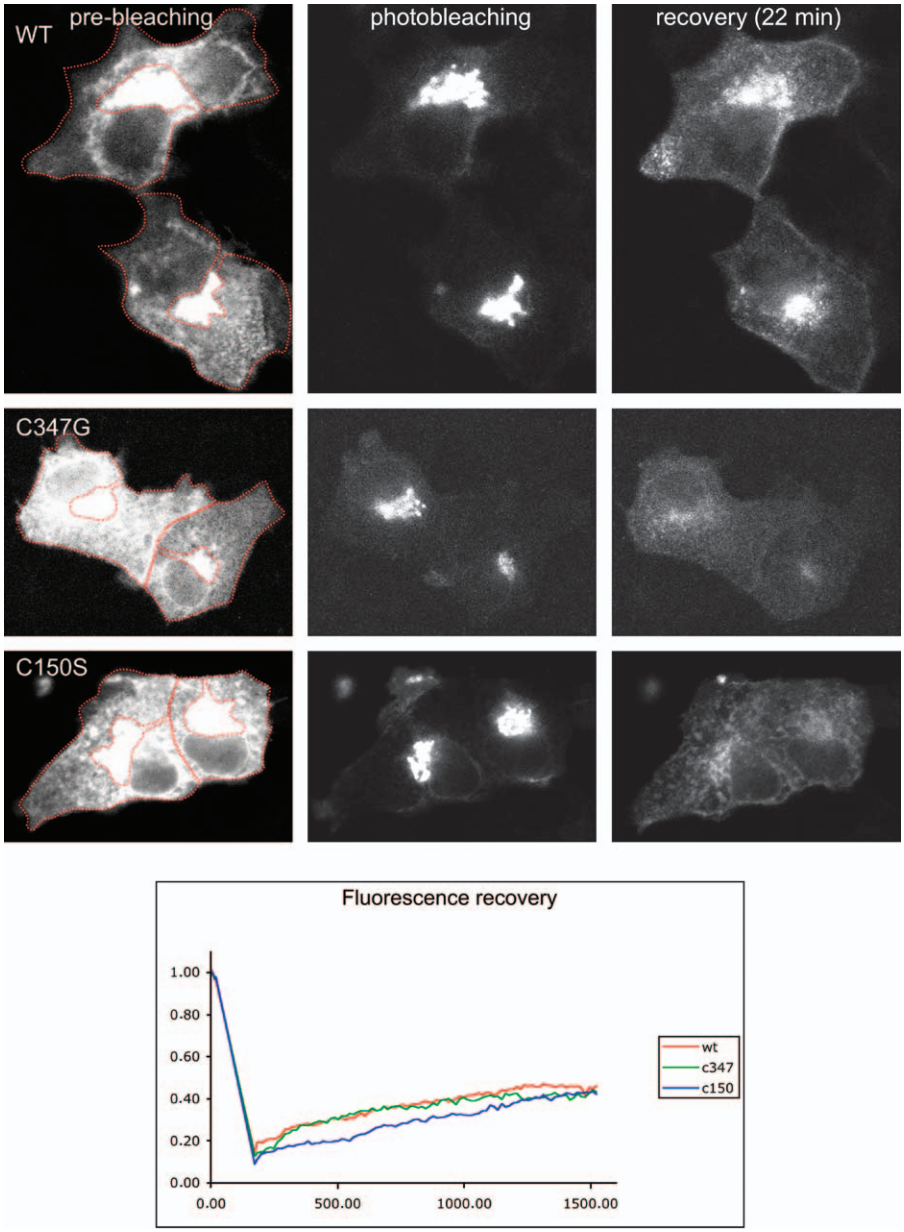

Figure 6: Time-lapse imaging of MDCK cells transiently transfected with either wt or mutant EGFP–uromodulin constructs. FRAP of the plasma membrane area is shown. Areas of photobleaching are indicated by the red dashed line. The graph below shows average fluorescence intensities in the region of interest after photobleaching (time-points every 5 seconds). Uromodulin mutations do not seem to alter TGN to plasma membrane trafficking.

cow uromodulin homologues, aspartic acid 59 being replaced by a serine in the cow sequence.

We assessed the effect of mutations by three different programs, SIFT (28), PMUT (29) and MUPRO (30), that allow accurate prediction in the absence of protein tertiary structure information. Although to different extent, all the analyzed mutations were predicted to destabilize the protein structure by at least one of the programs.

A common effect on protein trafficking could be clearly detected for all the mutations we investigated. By using FACS analysis, immunofluorescence and biochemical characterization, we were able to demonstrate partial retention in the ER of the mutant protein. Interestingly, different mutations seemed to impair protein trafficking to different extents. This difference was evident in several experiments, as shown, for instance, for mutants C150S and C347G (Figures 1B, 4–6), the former leading to a more severe cellular phenotype. Based on that, for some of the experimental conditions, we focused onto a subset of mutations that were representative of the different cellular phenotype severity. These results might reflect different *in vivo* effects of uromodulin mutations as already observed for other disease-associated proteins, e.g. podocin (33). However, based on the published clinical data of patients carrying the analyzed mutations, no clear phenotype to genotype correlation could be established.

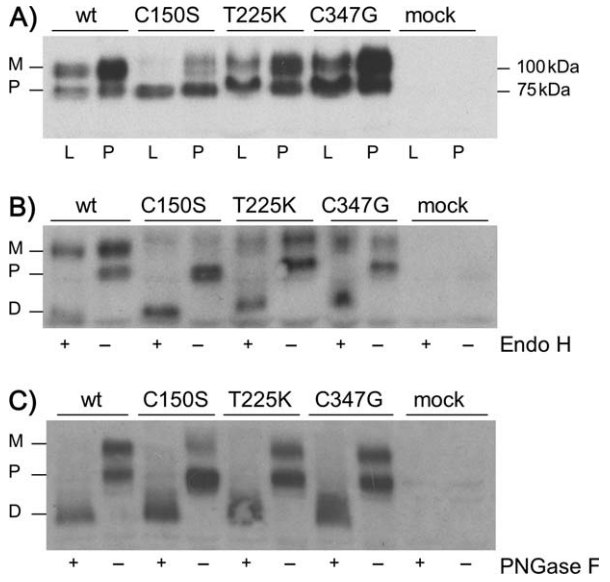

Figure 7: Western blot detection of wild type and mutant uromodulin in extracts of transiently transfected HEK293 cells. A) Western blot detection of uromodulin in the soluble (L) and insoluble (P) fractions of RIPA buffer extracts from transiently transfected HEK293 cells expressing either wt or mutant uromodulin. Uromodulin is found as a 100- and an 80-kDa isoform, corresponding to the mature (M) and a precursor (P) protein. B and C) Deglycosylation of uromodulin isoform. Cell extracts from wt and mutant uromodulin transfected cells were treated with endo-β-*N*-acetylglucosaminidase H (Endo H) (B) or peptide-N-glycosidase F (PNGase F) (C) and changes in molecular weight were visualized by Western blot. The 80-kDa uromodulin only is cleaved by Endo H to an about 60-kDa deglycosylated (D) isoforms. These data indicate that the 80-kDa isoform is an ER precursor that is enriched in the mutant transfected cell lysates.

Our results on wt uromodulin trafficking are consistent with previously published ones. In transiently transfected cells, the intracellular distribution of the protein was mainly localized in the Golgi, as clearly measured in EM experiments (Figure 3). This is consistent with previous findings in stably transfected HeLa cells, showing that intracellular [3H]mannose-labelled uromodulin was mainly separated as di- and trisialylated glycopeptides, suggesting that the protein accumulates in the distal Golgi compartments before being exposed at the cell surface (34).

A trafficking defect of mutant isoforms is consistent with previously published results, showing the presence of intracellular uromodulin aggregates in kidney biopsies from five patients (15,19), three of them carrying missense mutations not affecting cysteine residues. This finding underlies an early event in the disease progression, and it does not seem to be a mere consequence of advanced renal failure, as it was also reported in a patient first in his adolescence with a mild renal insufficiency (24). Uromodulin intracellular retention is also consistent with a dramatic reduction of protein levels in patient urine (15,19,35). Reduced protein excretion does not seem to be correlated to gender, age or glomerular filtration rate and seems to exceed the 50% expected one in the case of a heterozygous mutation, suggesting a possible dominant negative effect of mutant uromodulin in the tubule cells. However, no clear detrimental effect on wt protein trafficking could be observed when simulating the heterozygous state by transiently cotransfecting wt and mutant isoforms (15). Nonetheless, we cannot exclude that a dominant negative mechanism might require prolonged expression, i.e. expression of the two alleles in stably transfected cells.

Previous mass spectrometry experiments have shown that only wt uromodulin could be detected in urine samples from patients with established chronic renal failure (19), suggesting that mutant protein is entirely retained in tubular epithelial cells. Our results in transiently transfected HEK293 and MDCK cells are partly in contrast with these observations. Although differences between wt and mutant transfected cells can be appreciated with all the different experimental approaches that we undertook, we neither observed full retention of the mutant protein in the ER nor the formation of intracellular aggregates, as could be ascertained by immunofluorescence and EM analyses. Indeed, mutant protein isoforms could reach the plasma membrane and could be detected in the culture medium. Similar results were previously reported in stably transfected HEK293 and thick ascending limb of Henle's loop (TALH) cells where mutant uromodulin was transferred to the plasma membrane and released into the culture medium although less efficiently than the wt protein (36). These findings could reflect biases introduced by the *in vitro* systems, as high expression levels of the protein might saturate chaperone activity in the ER and the use of cell lines possibly having different secretory capacity compared with renal epithelial cells expressing uromodulin. However, we cannot exclude that mutant uromodulin could be detected when analyzing urine samples from presymptomatic patients with little, if any, impairment of renal function.

For the first time, we show that defective trafficking of mutant uromodulin is due to ER retention while protein GPI anchoring in the ER is not affected. Moreover, FRAP experiments showed that the export dynamics from the trans Golgi compartment to the plasma membrane is not affected. Indeed, uromodulin mutations did not seem to alter the glycosylation processes in the Golgi because Pi-PLC-purified and medium-purified mutant proteins that were treated with deglycosidases did not show any size difference when compared with the wt one. Of course, qualitative changes at a single *N*-glycan in mutant uromodulin cannot be excluded, and more in-depth studies would be needed to address this point.

Retention of the mutant uromodulin in the ER is very likely due to a common detrimental effect of mutations on protein tertiary structure and represents a key step in the

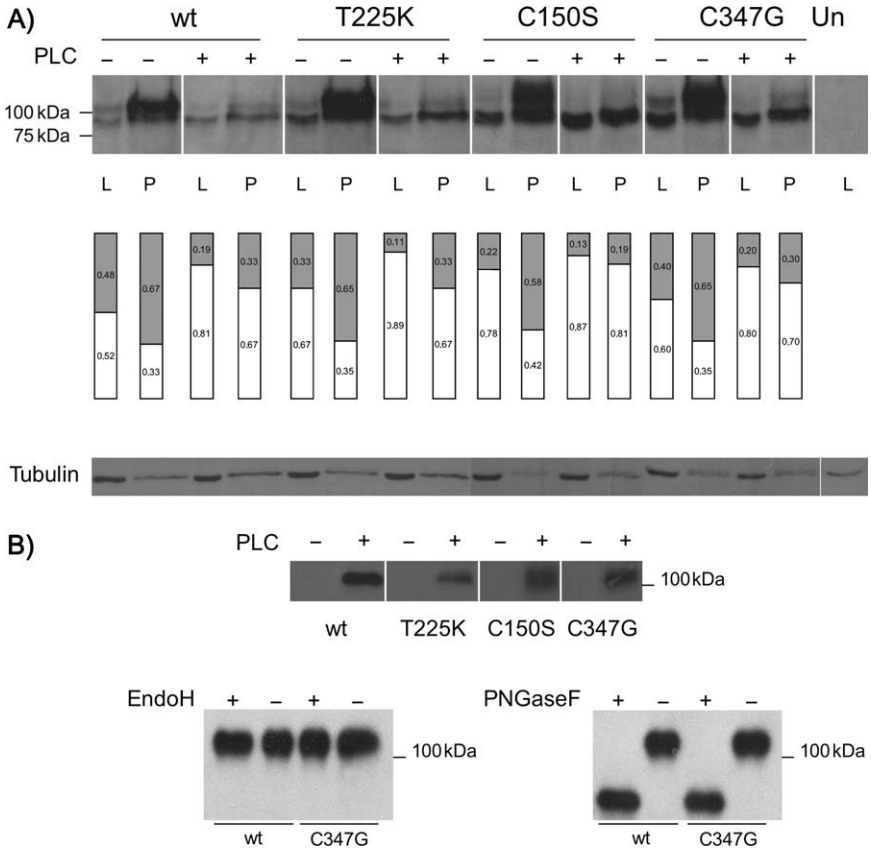

Figure 8: Western blot detection of wild type and mutant uromodulin after Pi-PLC treatment of transiently transfected HEK293 cells. A) Western blot detection of uromodulin in the soluble (L) and insoluble (P) fractions of RIPA buffer extracts from transiently transfected HEK293 cells expressing either wt or mutant uromodulin. In lanes marked with a +, cells were treated with Pi-PLC prior to cell extract preparation. Quantification of the ratio of mature (grey) to precursor (white) bands is shown below each lane. Pi-PLC treatment releases membrane-bound uromodulin both in wt and in mutant-expressing cells, suggesting that mutations do not alter GPI anchoring. Alpha-tubulin expression is shown as a loading control. B) Western blot analysis of Pi-PLC-cleaved uromodulin from wt and mutant transfected cells. Treatment with Endo H and PNGase F shows that Pi-PLC-cleaved wt and mutant uromodulin are of the mature type only. Un, untrasfected HEK293 cells.

pathogenesis of uromodulin-associated diseases. ER retention of misfolded mutant proteins has been described in several diseases (37,38), including kidney-affecting ones, as for aquaporin-2 in nephrogenic diabetes insipidus (39) and podocin in steroid-resistant nephrotic syndrome (33). In some cases, retained mutant protein is eventually retrotraslocated to the cytoplasm and degraded. However, in other conditions, the mutant protein can form aggregates that are accumulated either in the ER or in the cytoplasm (40). Perturbation of ER function can eventually lead to ER stress and activation of the unfolded protein response (UPR) pathway, a complex signalling network that upregulates ER chaperones and foldases and decreases the biosynthetic burden of the secretory pathway by downregulating expression of genes encoding secreted proteins (41). Alternatively, overload of the ER with mutant protein could activate the ER overload response (EOR), leading to activation of the nuclear transcription factor NFκB (42,43). Sustained activation of either EOR or UPR can eventually lead to cell death (44,45). It has been previously demonstrated that stable expression of two mutant uromodulin isoforms (H177–185del and C148Y) in HEK293 and TALH cells was associated to decreased protein secretion and increased apoptosis rate, particularly when cells were cultured in serum-free medium (36). This effect was partly rescued by treatment with colchicine and sodium 4-phenylbutyrate.

Cell response pathways that are elicited by mutant uromodulin retention are presently not known. Further experiments will be needed to characterize the toxicity of mutant protein expression in cell models and to understand its significance *in vivo*. It seems reasonable to hypothesize that accumulation of mutant uromodulin could lead to ER-stress-induced renal tubular cell death, eventually damaging kidney function and resulting in progressive renal failure.

In summary, we have reported a functional study of a panel of different uromodulin missense mutations characterizing protein processing in the secretory pathway. We showed that all mutations lead to trafficking defects due to retention in the ER. Mutant protein GPI anchoring to the membrane, modifications in the Golgi and TGN to plasma membrane transport were not affected. These data point at ER retention as a key event in the pathogenesis of uromodulin-associated diseases.

Materials and Methods

Uromodulin expression constructs and site-directed mutagenesis

Uromodulin full-length complementary DNA (cDNA) was cloned into the expression vector pcDNA3.1 (Invitrogen, Carlsbad, CA, USA) as previously described (15). Mutations in the uromodulin cDNA were introduced by the QuickChange site-directed mutagenesis kit (Stratagene, La Jolla, CA, USA).

We introduced the following mutations: 176A>T (codon GAT>GCT, D59A), 383A>G (codon AAT>AGT, N128S), 610C>G (codon CGC>GGC, R204G), 649T>C (codon TGC>CGC, C217R), 674C>A (codon ACG>AAG, T225K), 686T>G (codon ATG>AGG, M229R) and 707C>G (codon CCG>CGG, P236R) (Base number 1 corresponds to the first base of the translation start codon, AC NM_003361). The primer pairs used for site-directed mutagenesis are listed below (5′ to 3′):

- D59Af – GGGCTTCACCGGCGCTGGCCTGACCTGCGT
- D59Ar – ACGCAGGTCAGGCCAGCGCCGGTGAAGCCC
- N128Sf – CTGGCCACATGTGTCAGTGTGGTGGGCAGCTAC
- N128Sr – GTAGCTGCCCACCACACTGACACATGTGGCCAG
- R204Gf – CTGCGCGGCTGGTACGGCTTCGTGGGCCAGG
- R204Gr – CCTGGCCCACGAAGCAGTACCAGCCGCGCAG
- C217Rf – CGCATGGCCGAGACCCGCGTGCCAGTCCTGC
- C217Rr – GCAGGACTGGCACGCGGGTCTCGGCCATGCG
- T225Kf – TCCTGCGCTGCAACAAGGCCGCCCCCATGTG
- T225Kr – CACATGGGGGCGGCCTTGTTGCAGCGCAGGA
- M229Rf – ACACGGCCGCCCCCAGGTGGCTCAATGGCAC
- M229Rr – GTGCCATTGAGCCACCTGGGGGCGGCCGTGT
- P236Rf – GGCTCAATGGCACGCATCGGTCCAGCGACGAGGG
- P236Rr – CCCTCGTCGCTGGACCGATGCGTGCCATTGAGCC

Primers for site-directed mutagenesis for the mutations C148W, C150S, C315R, C317Y and C347G were previously published (15,23).

Uromodulin–EGFP fusion construct was obtained by amplifying EGFP cDNA with primers (EGFP-f, CTACCGGTGGTGTGAGCAAGGGCGAGGAGC; EGFP-r, CTACCGGTCTTGTACAGCTCGTCCATG). EGFP was then inserted into a newly created *Age*I site at position 78 in the uromodulin cDNA. The tag is inserted between threonine 26 and serine 27 in the protein sequence.

Constructs were fully resequenced before transfection experiments.

Newly reported mutation P236R was found in seven affected members of a FJHN Italian family (Brugnano and Scolari, personal communication).

Cell sorting experiments

Cell sorting experiments were carried out as previously reported (15). Briefly, transfections were carried out by Metafectene (Biontex, Munich, Germany) according to the manufacturer's instructions. We used 1 μg of plasmid DNA for 2.6×10^6 cells. Transfection efficiency was determined by cotransfecting with EGFP-expressing vector pcDNA3x(+)MyEGFP (Invitrogen). We changed media 2 h after transfection and let cells grow for 6–12 h. For cells cultured in reducing conditions, added media contained 1/2 mM DTT. Cells were collected in Versene (Invitrogen, USA) and resuspended in αMEM + FBS 2% (2.4×10^6 cells/mL). Cells were incubated with goat polyclonal antibody anti-uromodulin (1:1000/700 000 cells; ICN Biomedicals, Irvine, CA, USA) for 30 min at 4°C and washed with αMEM + FBS 2%. Cells were incubated for 30 min at 4°C with the secondary antibody: polyclonal donkey anti-goat antibody conjugated with Alexa 488 (1:2500/700.000 cells; Molecular Probes, Invitrogen, Carlsbad, CA, USA). Cells were washed with αMEM + FBS 2%, resuspended in 300 μL of αMEM + FBS 2% and incubated for 10 min at room temperature with 7-amino-actinomycin D for the exclusion of nonviable cells. Cell fluorescence was measured by flow cytometry (FACSCalibur; BD Biosciences, San Jose, CA, USA) and analyzed by CellQUEST software (BD Biosciences). Equal amount of total uromodulin produced in mutant and wt transfected cells was verified by Western blot analysis. Transfected cells were lysed 14 h after transfection in RadioImmunoPrecipitation Assay (RIPA) buffer [1% (Octylphenoxy)polyethoxyethanol (IGEPAL CA-630); Sigma-Aldrich, 50 mM Tris pH 7.4, 150 mM NaCl, 0.5% deoxycholate (DOC), 0.1% SDS, 2 mM ethylenediaminetetraacetic acid (EDTA), 0.5 mM phenylmethylsulphonyl fluoride (PMSF)]. Equal amount of protein (40 μg) was loaded onto reducing 8% SDS–PAGE. Western blot for uromodulin and alpha-tubulin was carried out as described below. Transfection efficiency was assessed by loading equal amount of protein extracts (30 μg) onto reducing 10% SDS–PAGE and by incubating transblotted PVDF membrane (Millipore, Billerica, MA, USA) with rabbit polyclonal antibody against green fluorescent protein (1:2000 dilution; Molecular Probes; Invitrogen) followed by incubation with horseradish-peroxidase-conjugated secondary antibody (1:5000 dilution; Promega, Madison, WI, USA).

Immunofluorescence experiments

Cells were grown for 16 h prior to transfection on glass cover slips in 12-well plates (Corning Life Sciences, Corning, NY, USA). Transfections were carried out as above using 500 ng of plasmid DNA for 10^6 cells. Fresh media were added 2 h after transfection. Cells were fixed at different times after transfection (4–6 h) either in 100% methanol for 5 min at −20°C (permeabilized cells) or in 4% paraformaldehyde (PFA) for 30 min at 37°C (unpermeabilized cells). Unpermeabilized and permeabilized cells were incubated with preimmune donkey serum for 30 min at 37°C. Cells were then incubated with goat polyclonal primary antibody against uromodulin (1:500 dilution; ICN Biomedicals). Permeabilized cells were also stained using sheep anti-giantin (1:300 dilution; Golgi marker; Covance Research Products, Berkeley, CA, USA) or rabbit anti-calreticulin (1:500 dilution; ER marker; Nventa, San Diego, CA, USA). We washed cells in phosphate-buffered saline solution and incubated with appropriate secondary antibodies (1:1000): AlexaFluor-594-conjugated donkey secondary antibody against goat immunoglobulin G (IgG) (Molecular Probes; Invitrogen) and Alexa-Fluor-488-conjugated donkey secondary antibody against sheep or rabbit IgG (Molecular Probes; Invitrogen). Unpermeabilized cells were incubated with tetramethylrhodamine B isothiocyanate (TRITC)-conjugated lectin (1:100 dilution; Sigma-Aldrich. We placed cells in fluorescent mounting medium (DakoCytomation, Glostrup, Denmark) over microscope slides and visualized them under confocal microscope Leica TCS SP2 AOBS (Leica Microsystems, Bannockburn, IL, USA).

Immuno-EM analysis

HEK293 cells were transfected using Lipofectamine 2000 (Invitrogen) with either wt or mutant uromodulin isoforms (500 ng of plasmid DNA for 10^6 cells), fixed with a mixture of 4% paraformaldehyde and 0.05% glutaraldehyde 6–8 h after transfection, labelled with goat polyclonal primary antibody against uromodulin (ICN Biomedicals) using the gold-enhance protocol, embedded in Epon-812 and cut as described previously (46). EM images were acquired from thin sections under a Philips Tecnai-12 electron microscope (Philips, Eindhoven, The Netherlands) using an ULTRA VIEW CCD digital camera. Thin sections were also used for quantification of gold particles residing within different compartments of the secretory pathway.

Time-lapse imaging

Time-lapse images were obtained using a Zeiss LSM510 confocal microscope system (Carl Zeiss, Gottingen, Germany). MDCK cells were transfected using Lipofectamine 2000 (Invitrogen) with either wt or mutant uromodulin–EGFP constructs (1 μg of plasmid DNA for 10^6 cells). MDCK cells expressing uromodulin–EGFP fusion proteins were observed at 37°C in 20 mM HEPES-buffered DMEM during the course of observation. For the ER to Golgi FRAP experiments, cells were analyzed 6 h after transfection. For the Golgi to plasma membrane FRAP experiments, cells were exposed to 20°C block 24 h after transfection to collect protein in the Golgi stacks. Fluorescence around the Golgi area was removed by selective photobleaching. Cells were then shifted from 20°C to 37°C in the presence of cycloheximide and therefore uromodulin–EGFP was allowed to leave the Golgi to the plasma membrane. Temperature was controlled with a Nevtek air stream stage incubator (Nevtek, Burnsville, VA, USA). EGFP molecules were excited with the 488-nm line of a krypton–argon laser and imaged with a 505–530 nm bandpass filter. Confocal digital images were collected at 15-second intervals using a Zeiss Plan-Neofluor 63× oil immersion objective (NA 1.4) with open pinhole to maintain the entire cell within the centre of the focal depth and thus to minimize changes in fluorescence. Selective photobleaching in regions of interest within the cell was carried out on the ZEISS LSM510 using 100 consecutive scans with a 488-nm laser line at full power. Average fluorescence intensities within regions of interests were quantified using LSM 3.2 software. The number of analyzed cells in the ER to Golgi experiments are 10 (wt, C347G) and 8 (C150S). The number of analyzed cells in the Golgi to plasma membrane experiments are eight (wt, C150S) and six (C347G).

Western blot

HEK293 cells transfection was carried out by Metafectene (Biontex) according to the manufacturer's instructions. We used 1 μg of plasmid DNA for 2.6×10^6 cells. We changed media 2 h after transfection and let cells grow for 24–48 h. Where indicated, cells were incubated with Pi-PLC digestion medium (DMEM + 20 mM Tris–Cl pH 7.4 + Pi-PLC 0.3 U/mL; Sigma-Aldrich) for 2 h in a 5% CO_2 atmosphere at 37°C. Cells were collected in Versene (Invitrogen) and lysed in RIPA buffer (1% IGEPAL CA-630; Sigma-Aldrich, 50 mM Tris pH 7.4, 150 mM NaCl, 0.5% DOC, 0.1% SDS, 2 mM EDTA and 0.5 mM PMSF). Where indicated, cell lysate and Pi-PLC digestion medium were treated with two different deglycosidases, peptide-N-glycosidase F (PNGase F; New England Biolabs, Beverly, MA, USA) and endo-β-*N*-acetylglucosaminidase H (Endo H; New England Biolabs) according to the manufacturer's protocol. Proteins were quantified by the Bio-Rad Protein Assay (Bio-Rad, Hercules, CA, USA). We loaded equal amounts of proteins (25 μg) onto reducing 8% SDS–PAGE. We incubated transblotted PVDF membranes (Millipore) with goat polyclonal antibody against uromodulin (1:1000 dilution; ICN Biomedicals) followed by incubation with horseradish-peroxidase-conjugated secondary antibody (1:2000 dilution; Promega). Anti-alpha-tubulin mouse monoclonal antibody was used as a loading control and to exclude cell lysis in the Pi-PLC digestion medium (1:2500 dilution; Molecular Probes; Invitrogen). Protein bands were visualized with the enhanced chemiluminescence kit (Amersham Biosciences, Piscataway, NJ, USA). When needed, quantification of the relative band intensities on the films was determined using a UVP ChemiDoc-IT Imaging System (UVP, Upland, CA, USA).

Prediction programs

PMUT (29) is available at http://mmb2.pcb.ub.es:8080/PMut. The effect of an amino acid substitution is predicted using only sequence-derived information (secondary structure, accessibility, evolutionary conservation, structure data and residue properties). All the derived information is input to a neural network that provides the final prediction on whether the target mutation is either pathological or neutral. The final output is always (i) a pathogenicity index ranging from 0 to 1 (indexes >0.5 signal pathological mutations) and (ii) a confidence index ranging from 0 (low) to 9 (high).

MUPRO (30) (http://www.ics.uci.edu/~baldig/mutation_intro.html) is a set of machine learning programs to predict how single-site amino acid mutation affects protein stability. We carried out the prediction of the value of energy change (ΔΔG) using support vector machine (recommended). If ΔΔG has a negative sign, a pathological effect of the mutation is predicted.

SIFT (28) (http://blocks.fhcrc.org/sift/SIFT.html) is based on the premise that protein evolution is correlated to protein function. Positions important for function should be conserved in an alignment of the protein family, whereas unimportant positions should appear diverse in an alignment. Amino acid changes with normalized probabilities less than 0.05 are predicted to be deleterious; those greater than or equal to 0.05 are predicted to be tolerated.

Acknowledgments

We thank Dr Francesca Boaretto and Dr Daniela Santon for their contribution to the functional characterization studies. We are grateful to Dr Rachele Brugnano for clinical investigation and for collection of biological samples of patients carrying the P236R mutation. L. R. is supported by Telethon-Italy (Grant TCP03018), Compagnia di San Paolo and Fondazione Cariplo (Grant CAR1520) and is an Assistant Telethon Scientist.

Supplementary Materials

Figure S1: Western blot detection of uromodulin and EGFP in extracts of transiently transfected cells. A) Western blot analysis of uromodulin in the soluble (L) and insoluble (P) fractions of RIPA buffer extracts from HEK293 cells transiently transfected with the EGFP-encoding plasmid pcDNA3x(+)MyEGFP and with either wt or mutant uromodulin. Cells were lysed 14 h after transfection. While the majority of uromodulin is detected as a mature form in the insoluble fraction for the wt, mutants are enriched in the immature form, mainly in the soluble fraction. Alpha-tubulin is shown as a loading control. B) Western blot analysis of EGFP as a control of transfection efficiency. Equal amounts of soluble fractions from (A) were loaded. Alpha-tubulin is shown as a loading control.

Figure S2: Intracellular distribution of different mutant uromodulin isoforms and giantin in transiently transfected HEK293 cells. A and B) Cells were transfected, methanol fixed 6 h after transfection and incubated with anti-uromodulin and anti-giantin (Golgi marker). Bar = 35 μm.

Figure S3: Intracellular distribution of different mutant uromodulin isoforms and calreticulin in transiently transfected HEK293 cells. A and B) Cells were transfected, methanol fixed 6 h after transfection and incubated with anti-uromodulin and anti-calreticulin (ER marker). Bar = 35 μm.

Figure S4: Immunofluorescence analysis showing plasma membrane distribution of wt and mutant uromodulin in transiently transfected HEK293 cells. Cells were transfected, PFA fixed 6 h after transfection (unpermeabilized cells) and incubated with anti-uromodulin and lectin-TRITC that was used to stain the plasma membrane. Bar = 35 μm.

Movie S1: Time-lapse video of MDCK cells expressing wt uromodulin–EGFP. Confocal digital images were collected at 15-second intervals for a duration of 20 min after selective photobleaching in the Golgi apparatus region.

Movie S2: Time-lapse video of MDCK cells expressing mutant (C150S) uromodulin–EGFP. Confocal digital images were collected at 15-second intervals for a duration of 20 min after selective photobleaching in the Golgi apparatus region.

Movie S3: Time-lapse video of MDCK cells expressing mutant (C347G) uromodulin–EGFP. Confocal digital images were collected at 15-second intervals for a duration of 20 min after selective photobleaching in the Golgi apparatus region.

Movie S4: Time-lapse video of MDCK cells expressing wt uromodulin–EGFP. Confocal digital images were collected at 15-second intervals for a duration of 25 min after selective photobleaching in the plasma membrane region.

Movie S5: Time-lapse video of MDCK cells expressing C150S uromodulin–EGFP. Confocal digital images were collected at 15-second intervals for a duration of 25 min after selective photobleaching in the plasma membrane region.

Movie S6: Time-lapse video of MDCK cells expressing C347G uromodulin–EGFP. Confocal digital images were collected at 15-second intervals for a duration of 25 min after selective photobleaching in the plasma membrane region.

Supplemental materials are available as part of the online article at http://www.blackwell-synergy.com

References

1. Serafini-Cessi F, Malagolini N, Cavallone D. Tamm-Horsfall glycoprotein: biology and clinical relevance. Am J Kidney Dis 2003;42:658–676.

2. Tamm I, Horsfall FL. Characterisation and separation of an inhibitor of viral hemagglutination present in urine. Proc Soc Exp Biol Med 1950;74:108–114.
3. Cavallone D, Malagolini N, Serafini-Cessi F. Mechanism of release of urinary Tamm-Horsfall glycoprotein from the kidney GPI-anchored counterpart. Biochem Biophys Res Commun 2001;280:110–114.
4. van Rooijen JJ, Voskamp AF, Kamerling JP, Vliegenthart JF. Glycosylation sites and site-specific glycosylation in human Tamm-Horsfall glycoprotein. Glycobiology 1999;9:21–30.
5. Fukuoka S, Kobayashi K. Analysis of the C-terminal structure of urinary Tamm-Horsfall protein reveals that the release of the glycosyl phosphatidylinositol-anchored counterpart from the kidney occurs by phenylalanine-specific proteolysis. Biochem Biophys Res Commun 2001;289:1044–1048.
6. Bachmann S, Koeppen-Hagemann I, Kriz W. Ultrastructural localization of Tamm-Horsfall glycoprotein (THP) in rat kidney as revealed by protein A-gold immunocytochemistry. Histochemistry 1985;83: 531–538.
7. Mattey M, Naftalin L. Mechanoelectrical transduction, ion movement and water stasis in uromodulin. Experientia 1992;48:975–980.
8. Bates JM, Raffi HM, Prasadan K, Mascarenhas R, Laszik Z, Maeda N, Hultgren SJ, Kumar S. Tamm-Horsfall protein knockout mice are more prone to urinary tract infection: rapid communication. Kidney Int 2004;65:791–797.
9. Mo L, Zhu XH, Huang HY, Shapiro E, Hasty DL, Wu XR. Ablation of the Tamm-Horsfall protein gene increases susceptibility of mice to bladder colonization by type 1-fimbriated Escherichia coli. Am J Physiol Renal Physiol 2004;286:F795–F802.
10. Raffi HS, Bates JM Jr, Laszik Z, Kumar S. Tamm-Horsfall protein acts as a general host-defense factor against bacterial cystitis. Am J Nephrol 2005;25:570–578.
11. Mo L, Huang HY, Zhu XH, Shapiro E, Hasty DL, Wu XR. Tamm-Horsfall protein is a critical renal defense factor protecting against calcium oxalate crystal formation. Kidney Int 2004;66:1159–1166.
12. Saemann MD, Weichhart T, Zeyda M, Staffler G, Schunn M, Stuhlmeier KM, Sobanov Y, Stulnig TM, Akira S, von Gabain A, von Ahsen U, Horl WH, Zlabinger GJ. Tamm-Horsfall glycoprotein links innate immune cell activation with adaptive immunity via a Toll-like receptor-4-dependent mechanism. J Clin Invest 2005;115:468–475.
13. Saemann MD, Weichhart T, Horl WH, Zlabinger GJ. Tamm-Horsfall protein: a multilayered defence molecule against urinary tract infection. Eur J Clin Invest 2005;35:227–235.
14. Hart TC, Gorry MC, Hart PS, Woodard AS, Shihabi Z, Sandhu J, Shirts B, Xu L, Zhu H, Barmada MM, Bleyer AJ. Mutations of the UMOD gene are responsible for medullary cystic kidney disease 2 and familial juvenile hyperuricaemic nephropathy. J Med Genet 2002;39:882–892.
15. Rampoldi L, Caridi G, Santon D, Boaretto F, Bernascone I, Lamorte G, Tardanico R, Dagnino M, Colussi G, Scolari F, Ghiggeri GM, Amoroso A, Casari G. Allelism of MCKD, FJHN and GCKD caused by impairment of uromodulin export dynamics. Hum Mol Genet 2003; 12:3369–3384.
16. Lens XM, Banet JF, Outeda P, Barrio-Lucia V. A novel pattern of mutation in uromodulin disorders: autosomal dominant medullary cystic kidney disease type 2, familial juvenile hyperuricemic nephropathy, and autosomal dominant glomerulocystic kidney disease. Am J Kidney Dis 2005;46:52–57.
17. Bleyer AJ, Trachtman H, Sandhu J, Gorry MC, Hart TC. Renal manifestations of a mutation in the uromodulin (Tamm Horsfall protein) gene. Am J Kidney Dis 2003;42:E20–E26.
18. Turner JJ, Stacey JM, Harding B, Kotanko P, Lhotta K, Puig JG, Roberts I, Torres RJ, Thakker RV. Uromodulin mutations cause familial juvenile hyperuricemic nephropathy. J Clin Endocrinol Metab 2003;88: 1398–1401.
19. Dahan K, Devuyst O, Smaers M, Vertommen D, Loute G, Poux JM, Viron B, Jacquot C, Gagnadoux MF, Chauveau D, Buchler M, Cochat P, Cosyns JP, Mougenot B, Rider MH, *et al.* A cluster of mutations in the UMOD gene causes familial juvenile hyperuricemic nephropathy with abnormal expression of uromodulin. J Am Soc Nephrol 2003;14: 2883–2893.
20. Hodanova K, Kalbacova M, Stiburkova B, Majewski J, Marinaki A, Simmonds HA, Matthijs G, Fryns JP, Ott J, Kmoch S. Familial juvenile hyperuricemic nephropathy (FJHN): linkage analysis in 17 families, transcriptional characterization of the FJHN critical region on chromosome 16p11.2 and the analyses of uromodulin and other candidate genes. Am J Hum Genet 2003;73:565 (Poster 2324).
21. Wolf MT, Mucha BE, Attanasio M, Zalewski I, Karle SM, Neumann HP, Rahman N, Bader B, Baldamus CA, Otto E, Witzgall R, Fuchshuber A, Hildebrandt F. Mutations of the uromodulin gene in MCKD type 2 patients cluster in exon 4, which encodes three EGF-like domains. Kidney Int 2003;64:1580–1587.
22. Kudo E, Kamatani N, Tezuka O, Taniguchi A, Yamanaka H, Yabe S, Osabe D, Shinohara S, Nomura K, Segawa M, Miyamoto T, Moritani M, Kunika K, Itakura M. Familial juvenile hyperuricemic nephropathy: detection of mutations in the uromodulin gene in five Japanese families. Kidney Int 2004;65:1589–1597.
23. Tinschert S, Ruf N, Bernascone I, Sacherer K, Lamorte G, Neumayer HH, Nurnberg P, Luft FC, Rampoldi L. Functional consequences of a novel uromodulin mutation in a family with familial juvenile hyperuricaemic nephropathy. Nephrol Dial Transplant 2004;19: 3150–3154.
24. Bleyer AJ, Hart TC, Willingham MC, Iskandar SS, Gorry MC, Trachtman H. Clinico-pathologic findings in medullary cystic kidney disease type 2. Pediatr Nephrol 2005;20:824–827.
25. Calado J, Gaspar A, Clemente C, Rueff J. A novel heterozygous missense mutation in the UMOD gene responsible for familial juvenile hyperuricemic nephropathy. BMC Med Genet 2005;6:5.
26. Yang H, Wu C, Zhao S, Guo J. Identification and characterization of D8C, a novel domain present in liver-specific LZP, uromodulin and glycoprotein 2, mutated in familial juvenile hyperuricaemic nephropathy. FEBS Lett 2004;578:236–238.
27. Jovine L, Darie CC, Litscher ES, Wassarman PM. Zona pellucida domain proteins. Annu Rev Biochem 2005;74:83–114.
28. Ng PC, Henikoff S. SIFT: predicting amino acid changes that affect protein function. Nucleic Acids Res 2003;31:3812–3814.
29. Ferrer-Costa C, Gelpi JL, Zamakola L, Parraga I, de la Cruz X, Orozco M. PMUT: a web-based tool for the annotation of pathological mutations on proteins. Bioinformatics 2005;21:3176–3178.
30. Cheng J, Randall A, Baldi P. Prediction of protein stability changes for single-site mutations using support vector machines. Proteins 2006;62: 1125–1132.
31. Fletcher AP, Neuberger A, Ratcliffe WA. Tamm-Horsfall urinary glycoprotein. The chemical composition. Biochem J 1970;120: 417–424.
32. Downing AK, Knott V, Werner JM, Cardy CM, Campbell ID, Handford PA. Solution structure of a pair of calcium-binding epidermal growth factor-like domains: implications for the Marfan syndrome and other genetic disorders. Cell 1996;85:597–605.
33. Roselli S, Moutkine I, Gribouval O, Benmerah A, Antignac C. Plasma membrane targeting of podocin through the classical exocytic pathway: effect of NPHS2 mutations. Traffic 2004;5:37–44.
34. Malagolini N, Cavallone D, Serafini-Cessi F. Intracellular transport, cell-surface exposure and release of recombinant Tamm-Horsfall glycoprotein. Kidney Int 1997;52:1340–1350.
35. Bleyer AJ, Hart TC, Shihabi Z, Robins V, Hoyer JR. Mutations in the uromodulin gene decrease urinary excretion of Tamm-Horsfall protein. Kidney Int 2004;66:974–977.

36. Choi SW, Ryu OH, Choi SJ, Song IS, Bleyer AJ, Hart TC. Mutant Tamm-Horsfall glycoprotein accumulation in endoplasmic reticulum induces apoptosis reversed by colchicine and sodium 4-phenylbutyrate. J Am Soc Nephrol 2005;16:3006–3014.
37. Aridor M, Hannan LA. Traffic jams II: an update of diseases of intracellular transport. Traffic 2002;3:781–790.
38. Aridor M, Hannan LA. Traffic jam: a compendium of human diseases that affect intracellular transport processes. Traffic 2000;1:836–851.
39. Mulders SM, Knoers NV, Van Lieburg AF, Monnens LA, Leumann E, Wuhl E, Schober E, Rijss JP, Van Os CH, Deen PM. New mutations in the AQP2 gene in nephrogenic diabetes insipidus resulting in functional but misrouted water channels. J Am Soc Nephrol 1997;8: 242–248.
40. Kopito RR, Sitia R. Aggresomes and Russell bodies. Symptoms of cellular indigestion? EMBO Rep 2000;1:225–231.
41. Schroder M, Kaufman RJ. ER stress and the unfolded protein response. Mutat Res 2005;569:29–63.
42. Lawless MW, Greene CM, Mulgrew A, Taggart CC, O'Neill SJ, McElvaney NG. Activation of endoplasmic reticulum-specific stress responses associated with the conformational disease Z alpha 1-antitrypsin deficiency. J Immunol 2004;172:5722–5726.
43. Pahl HL. Signal transduction from the endoplasmic reticulum to the cell nucleus. Physiol Rev 1999;79:683–701.
44. Nakagawa T, Zhu H, Morishima N, Li E, Xu J, Yankner BA, Yuan J. Caspase-12 mediates endoplasmic-reticulum-specific apoptosis and cytotoxicity by amyloid-beta. Nature 2000;403:98–103.
45. Kuang E, Wan Q, Li X, Xu H, Liu Q, Qi Y. ER Ca2+ depletion triggers apoptotic signals for endoplasmic reticulum (ER) overload response induced by overexpressed reticulon 3 (RTN3/HAP). J Cell Physiol 2005;204:549–559.
46. Polishchuk EV, Di Pentima A, Luini A, Polishchuk RS. Mechanism of constitutive export from the golgi: bulk flow via the formation, protrusion, and en bloc cleavage of large trans-golgi network tubular domains. Mol Biol Cell 2003;14:4470–4485.